ADVANCED MATERIALS
www.advmat.de

Thinnest Nonvolatile Memory Based on Monolayer h-BN

Xiaohan Wu, Ruijing Ge, Po-An Chen, Harry Chou, Zhepeng Zhang, Yanfeng Zhang, Sanjay Banerjee, Meng-Hsueh Chiang, Jack C. Lee, and Deji Akinwande**

2D materials have attracted much interest over the past decade in nanoelectronics. However, it was believed that the atomically thin layered materials are not able to show memristive effect in vertically stacked structure, until the recent discovery of monolayer transition metal dichalcogenide (TMD) atomristors, overcoming the scaling limit to sub-nanometer. Herein, the nonvolatile resistance switching (NVRS) phenomenon in monolayer hexagonal boron nitride (h-BN), a typical 2D insulator, is reported. The h-BN atomristors are studied using different electrodes and structures, featuring forming-free switching in both unipolar and bipolar operations, with large on/off ratio (up to 10^7). Moreover, fast switching speed (<15 ns) is demonstrated via pulse operation. Compared with monolayer TMDs, the one-atom-thin h-BN sheet reduces the vertical scaling to ≈0.33 nm, representing a record thickness for memory materials. Simulation results based on ab-initio method reveal that substitution of metal ions into h-BN vacancies during electrical switching is a likely mechanism. The existence of NVRS in monolayer h-BN indicates fruitful interactions between defects, metal ions and interfaces, and can advance emerging applications on ultrathin flexible memory, printed electronics, neuromorphic computing, and radio frequency switches.

2D materials have attracted much attention for next-generation electron devices, optoelectronics, flexible electronics, and bioelectronics.[1–5] In the last few years, nonvolatile resistance switching (NVRS) behavior has been observed in various 2D materials, including graphene oxide, solution-processed transition metal dichalcogenides (TMDs), chemical vapor deposition (CVD) grown MoS_2 in lateral devices, and degraded black phosphorus, in which the resistance can be switched between a high resistance state (HRS) and a low resistance state (LRS) via external electrical bias.[6–10] Due to the excessive leakage current, monolayer 2D materials were not believed to have NVRS effect in vertical metal–insulator–metal (MIM) configuration.[11,12] However, the demonstration of single-layer TMD-based atomristors (memristive effect in atomic sheets) overturned the traditional view, scaling down the active material thickness to ≈0.7 nm.[13,14]

Unlike graphene (semimetal) or TMDs (semiconductor), hexagonal boron nitride (h-BN), a typical 2D insulator material, was mostly used as a dielectric or substrate material, owing to its large band gap and outstanding thermal characteristics.[15–20] Recently, Lanza and co-workers reported the resistance switching phenomenon in multilayer h-BN, featuring the coexistence of both bipolar (nonvolatile) and threshold (volatile) switching.[21,22] In this article, we report the observation of NVRS effect in monolayer h-BN vertically sandwiched by metallic electrodes. The single-layer h-BN based atomristors show stable bipolar and unipolar nonvolatile switching, with forming-free characteristic and large on/off current ratio (up to 10^7). Two different device structures (crossbar devices, and litho- and transfer-free devices) using three metallic electrodes (Au, Ni, and Ag) have been studied. Furthermore, taking advantage of the ultrathin active layer, fast switching speed (<15 ns) is demonstrated via pulse operation. Ab-initio simulation reveals favorable substitution of metal ions into boron or nitrogen vacancies, which corresponds to the switching from HRS to LRS, indicative of a conductive-bridge-like mechanism. The realization of one-atom-thin h-BN NVRS devices not only expands the family of atomristors to 2D insulators, but also improves the thickness record from ≈0.65 nm (monolayer TMDs) to ≈0.33 nm (monolayer h-BN). Our work indicates a potentially universal memory effect in various 2D insulating monolayers for applications including high-density data storage arrays, neuromorphic computing, flexible electronics, and zero-power radio frequency (RF) switches.

Continuous monolayer h-BN atomic sheets were grown on Au or Ni foils via CVD. The metal foils can be used as global

X. Wu, R. Ge, P.-A. Chen, Dr. H. Chou, Prof. S. Banerjee, Prof. J. C. Lee, Prof. D. Akinwande
Microelectronics Research Center
University of Texas at Austin
Austin, TX 78758, USA
E-mail: leejc@austin.utexas.edu; deji@ece.utexas.edu
P.-A. Chen, Prof. M.-H. Chiang
Institute of Microelectronics
Department of Electrical Engineering
National Cheng Kung University
Tainan 701, Taiwan
Z. Zhang, Prof. Y. Zhang
Department of Materials Science and Engineering
College of Engineering
Peking University
Beijing 100871, China
The ORCID identification number(s) for the author(s) of this article can be found under https://doi.org/10.1002/adma.201806790.

DOI: 10.1002/adma.201806790

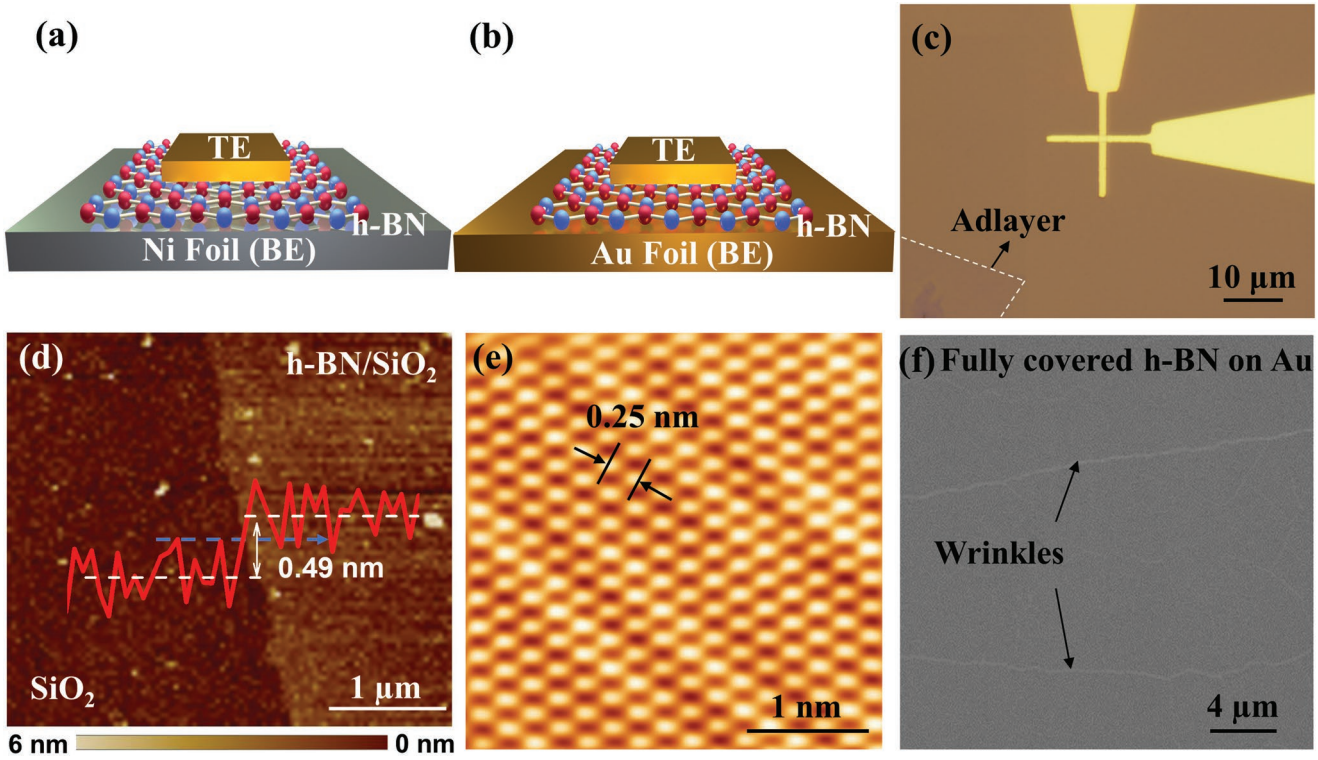

Figure 1. Schematic, device and material characterization. The schematics of monolayer h-BN lithography-free and *transfer*-free MIM sandwich structure based on a) Ni foil and b) Au foil. Transferred h-BN MIM devices were also investigated as shown in c) optical image of fabricated h-BN crossbar with Au electrodes. d) AFM images of transferred samples. Inset: the height profile analysis yields an average step in height of ≈0.49 nm relative to the substrate, suggesting monolayer h-BN. e) Atomic resolution STM image of as-grown samples, which shows the representative honeycomb structure of h-BN with a lattice constant of ≈0.25 nm, indicating the formation of a high-quality h-BN layer on Au foil. f) SEM images of as-grown samples on Au foil indicating full coverage with monolayer CVD-grown h-BN films. The wrinkles are due to the thermal expansion difference between Au foil and h-BN film.

bottom electrodes (BEs), while top electrodes (TEs) were directly deposited on the h-BN thin film through laser shadow mask. Note that there is no transfer nor lithography process involved in the device preparation on metal substrates. Thus, the effect of chemical residues due to the two processes can be eliminated. The devices are labeled as litho- and transfer-free atomristors and illustrated in **Figure 1**a,b. To achieve small-scale devices (below μm^2), crossbar devices were fabricated as shown in Figure 1c. The monolayer h-BN sheets were transferred onto SiO_2/Si substrates with BE, then followed with the deposition of TE. As an inert metal, gold electrodes were utilized to rule out the possible influence of metal oxide at the interface. Atomic force microscopy (AFM) was conducted to confirm the monolayer nature of transferred h-BN films on Si/SiO_2 substrate (see Figure 1d). In addition, atomic resolution scanning tunneling microscope (STM), Figure 1e, shows the representative honeycomb structure of as-grown h-BN on Au foil with a lattice constant of ≈ 0.25 nm, suggesting the high quality of the atomically thin sheets. Scanning electron microscope (SEM) image is presented as Figure 1f, indicating full coverage of CVD-grown single-layer h-BN on Au foil. X-ray photoelectron spectroscopy (XPS) and Raman were performed as well to characterize the h-BN film, which is included in Supporting Information as Figures S1 and S2 in the Supporting Information.

The fabricated atomristors were electrically tested using DC voltage sweep under ambient conditions, showing NVRS behavior in both crossbar and litho- and transfer-free devices. **Figure 2**a displays a representative bipolar *I–V* curve of a crossbar Au/monolayer h-BN/Au atomristor. The pristine device is initially at HRS, until a positive bias (≈3 V in this case) is applied to switch the device to LRS, which is commonly referred to as a "SET" process. The atomristor will remain at LRS without power consumption. To switch back to HRS, a negative bias (≈−1 V in this case) is applied on the device, which is known as the "RESET" process. A large on/off current ratio up to 10^7 can normally be achieved through the resistance switching. Some of the devices can even reach the on/off ratio of 10^8, as shown in Figure S3 in the Supporting Information. Being similar to the previous report on monolayer TMD-based atomristors,[13] no electro-forming process is required for the h-BN NVRS devices, possibly due to the simplicity of conductive path formation in the ultrathin monolayer. Unipolar resistance switching (SET and RESET voltages are achieved with the same polarity) is also observed in h-BN atomristors (Figure 2b). To rule out the effect of polymer residues introduced by transfer and e-beam lithography for crossbar atomristors, litho- and transfer-free devices were fabricated and tested. The *I–V* curves of the residue-free devices show resistance switching behavior on Au and Ni foils (see Figure 2c,d), indicating that nonvolatile memory effect is an intrinsic property of monolayer h-BN. Note that while both Au and Ni electrodes were used in this study, various inert or active metals are also

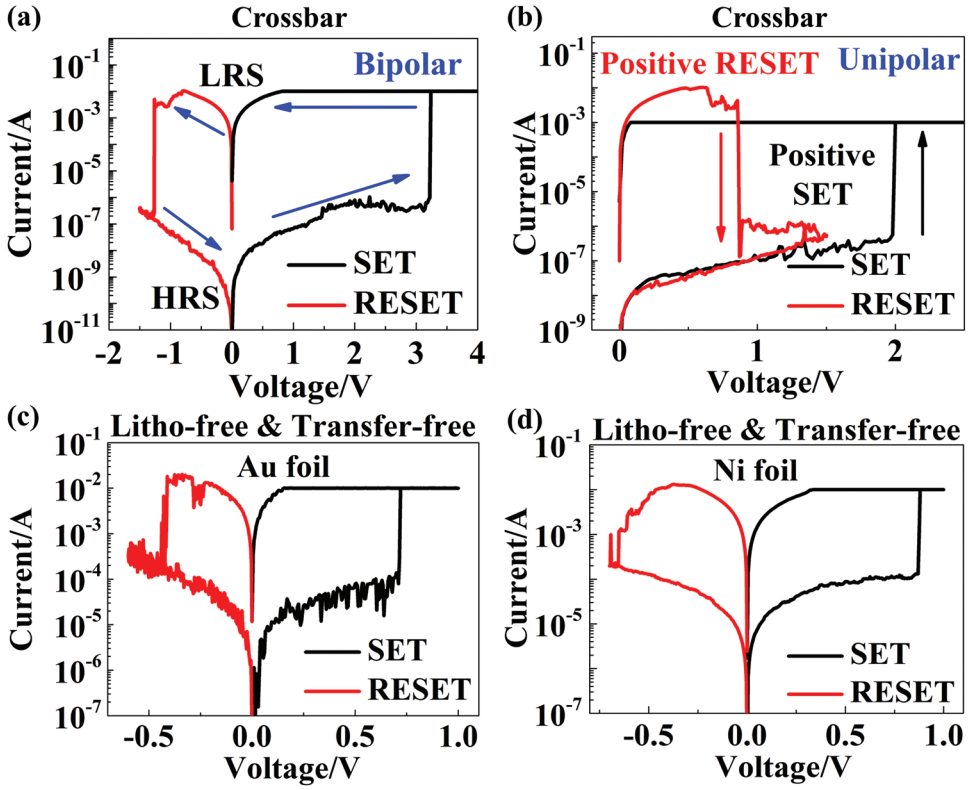

Figure 2. Typical *I–V* curves of monolayer h-BN MIM devices. Representative *I–V* curve of a) bipolar and b) unipolar resistive switching behavior in monolayer h-BN crossbar device with lateral area of $1 \times 1\ \mu m^2$. For unipolar operation, both SET and RESET transitions are achieved under positive bias. Representative *I–V* curves of resistive switching behavior in monolayer h-BN litho-free and transfer-free MIM devices based on c) Au foil and d) Ni foil.

expected to be suitable opening the design space for further research in electrode and interface engineering.

To investigate the mechanism of resistance switching behavior in monolayer h-BN, the low-voltage "read" *I–V* characteristics at LRS (**Figure 3**a) and HRS (Figure 3b,c) are studied at various temperatures. For the LRS profiles, the current decreases as the temperature increases, which is a signature of metallic conduction. The linear *I–V* relationship, together with the calculated normalized conductance $G_n = (dI/dV)/(I/V) = 1$, is consistent with Ohmic conduction. Compared with the monolayer TMD counterpart,[13] the h-BN atomristors show the same electron transport mechanism at LRS; while at HRS, the nonlinear *I–V* characteristics reveal a different mechanism. As shown in Figure 3b, the current increases as the temperature increases. Among various transport models considered, the HRS data are best-fitted by the Poole–Frenkel emission model as shown below (Equation (1))[23,24]

$$J \propto E \exp\left[\frac{-q\left(\phi_T - \sqrt{qE/\pi\varepsilon_r\varepsilon_0}\right)}{kT}\right] \quad (1)$$

where J is the current density, T is the absolute temperature, q is the electronic charge, $q\varphi_T$ is the trap energy level, E is the electric field across the h-BN layer, k is Boltzmann's constant, ε_0 is the permittivity in vacuum, and ε_r is the optical dielectric constant. The fitted results indicate that trapping states are involved in the electron transportation at HRS. Considering the structure of monolayer h-BN, boron vacancies are energetically favorable and may serve as the localized trapping centers for electrons. While at LRS, the boron vacancies can be substituted by metal ions, leading to a more conductive Ohmic transport through the links formed by the metal atoms.

The switching mechanisms are further supported by ab-initio simulation results. From defect studies, boron or nitrogen vacancies commonly exist in h-BN sheets and have significant influence on the electron conduction.[21,25,26] The simulated initial configuration consists of a single-layer h-BN sheet with a boron vacancy and a positive gold ion is placed over the sheet (see Figure 3d). After the optimization process, the positively charged gold ion is reduced at the boron vacancy, and then chemisorbs on the h-BN layer, which is shown as the final state in Figure 3e. Similarly, negatively charged gold ion with boron vacancy is investigated. However, no movement of the ion is observed during the optimization process, which indicates that positive ions are energetically preferable for substitution. Moreover, nitrogen vacancies are also studied with positive and negative gold ions. The simulation results, consistent with the boron vacancies case, show that positive ions tend to substitute into the nitrogen vacancy, while negative ions appear dormant. Animated images of the four cases are presented in Figure S4 in the Supporting Information. Furthermore, we calculated the energies for gold ion stably occupying boron or nitrogen vacancy as shown in Table S2 in the Supporting Information. The calculation details can be found in supporting information. According to the calculation results, the energies of different charged gold follows that Au (–1) > Au (neutral) > Au(+1). Thus,

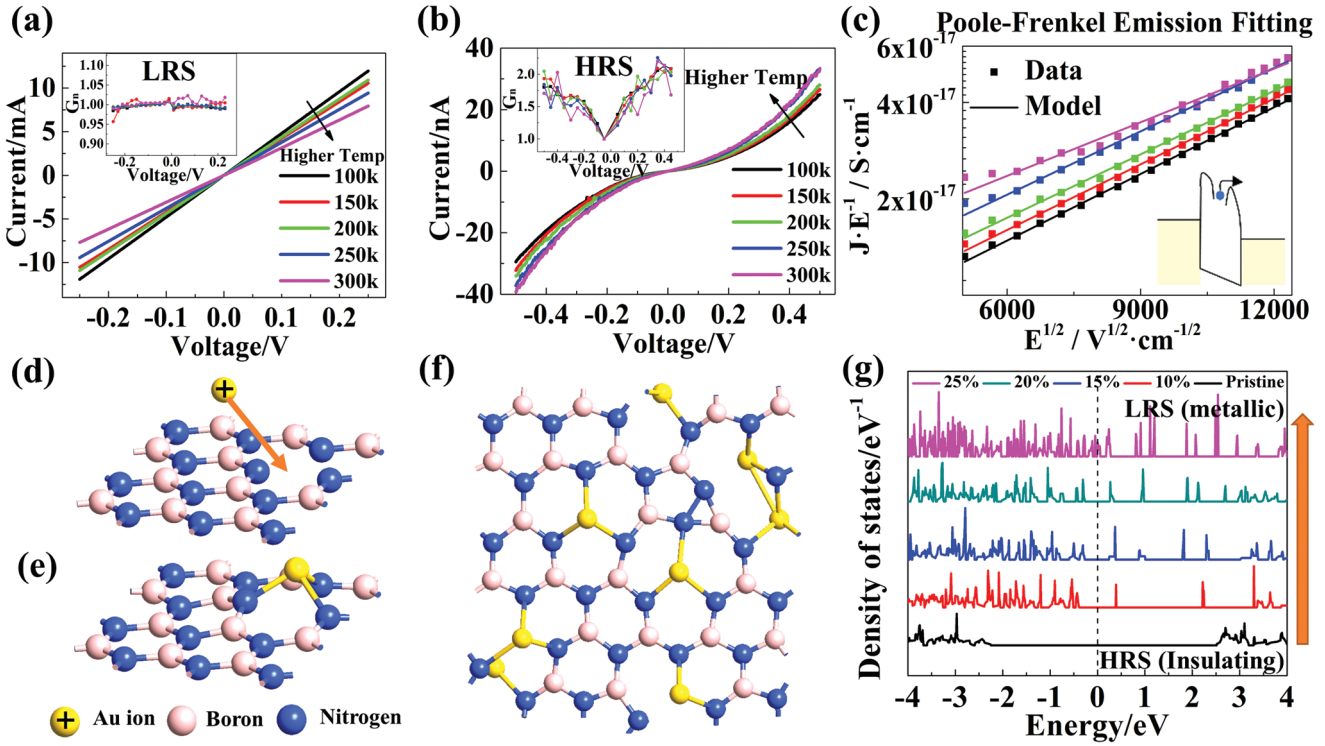

Figure 3. Dependence of temperature and compliance current. a) The "READ" *I–V* characteristics at LRS based on h-BN crossbar devices at different temperatures indicating a metallic character (temperature legend is in part b). The inset shows the normalized conductance G_n and the schematic of proposed mechanism based on Ohmic direct tunneling via defect(s) at LRS. b) The "READ" *I–V* characteristics at HRS at different temperatures. The current increases as the temperature increases. The inset shows the normalized conductance G_n. c) Fitted data using Poole–Frenkel model for HRS. The inset shows the schematic of the model. The ab-initio simulation results of d) the initial states and e) the final state of optimization process for gold ion and boron vacancies in monolayer h-BN. The results show that the gold ion tends to substitute into the boron vacancies, possibly resulting in the conductive bridge formation and SET process. f) An illustration for density of states calculation, where 25% boron atoms are replaced by gold atoms. g) Density of states for different gold replacement percentage of boron (dash line: Fermi level). The results indicate a switching to LRS at high gold replacement percentage.

the positive Au ion is the most favorable in the adsorption process, which is consistent with the animated images in Figure S4 in the Supporting Information. In addition, the adsorption with boron vacancy generally has lower energy than the one with nitrogen vacancy. Thus, the boron vacancy is more likely to be replaced with Au. It is worthwhile to notice that the positively charged gold ion adsorption on boron vacancy shows the lowest energy, which means it is the most stable case among our calculation settings.[21] The simulation results for charged vacancies are also shown in Figure S5 in the Supporting Information. In order to further verify the existence of localized conductive path, a small h-BN system is studied with different ratios of gold ions replacing the boron vacancies (Figure 3f as an example). Based on the density of states calculation (Figure 3g), the band gap of the monolayer h-BN shrinks as the replacement percentage increases. At high percentage, the Fermi level is embedded within the induced states, indicating a switching to LRS with metallic character. The occupation of the metal ions into boron vacancies suggests a local conductive-bridge-like mechanism in the MIM sandwich. It can be inferred that at HRS, electrons transport through the h-BN film with boron vacancies on it, where the boron vacancies serve as trapping centers, leading to a Poole–Frenkel conduction as mentioned above. During the SET process, the gold atoms located at the positive biased electrodes lose their electrons and become positively charged gold ions ($Au \rightarrow Au^+ + e^-$). Then, the ions are attracted by the boron vacancies and subsequently reduced ($Au^+ + e^- \rightarrow Au$), forming a conductive path in the vertical direction to establish the LRS. Area-dependence characteristics are analyzed (shown in Figure S6, Supporting Information), which further proves the conductive-bridge-like behavior for resistance switching in h-BN monolayer. It is worth noting that the underlying mechanisms regarding polarity (the competition between bipolar and unipolar) are expected to benefit from subsequent simulation works based on ab-initio method with the consideration of external bias.

One straightforward application of atomristors is nonvolatile memory devices, since the resistance states can be switched cyclically and retained without power supply. Beyond DC characterization, pulse SET/RESET is feasible for monolayer h-BN atomristors (see **Figure 4**a,b). The read *I–V* curves before and after applying pulses clearly show the switching from OFF state to ON state (SET process in Figure 4a) and from ON state to OFF state (RESET process in Figure 4b), with 15 ns SET switching speed, and 50 ns RESET switching speed (detailed process of pulse operation can be found in Figure S7, Supporting Information). Preliminary reliability tests have been conducted, showing stable switching characteristics. The

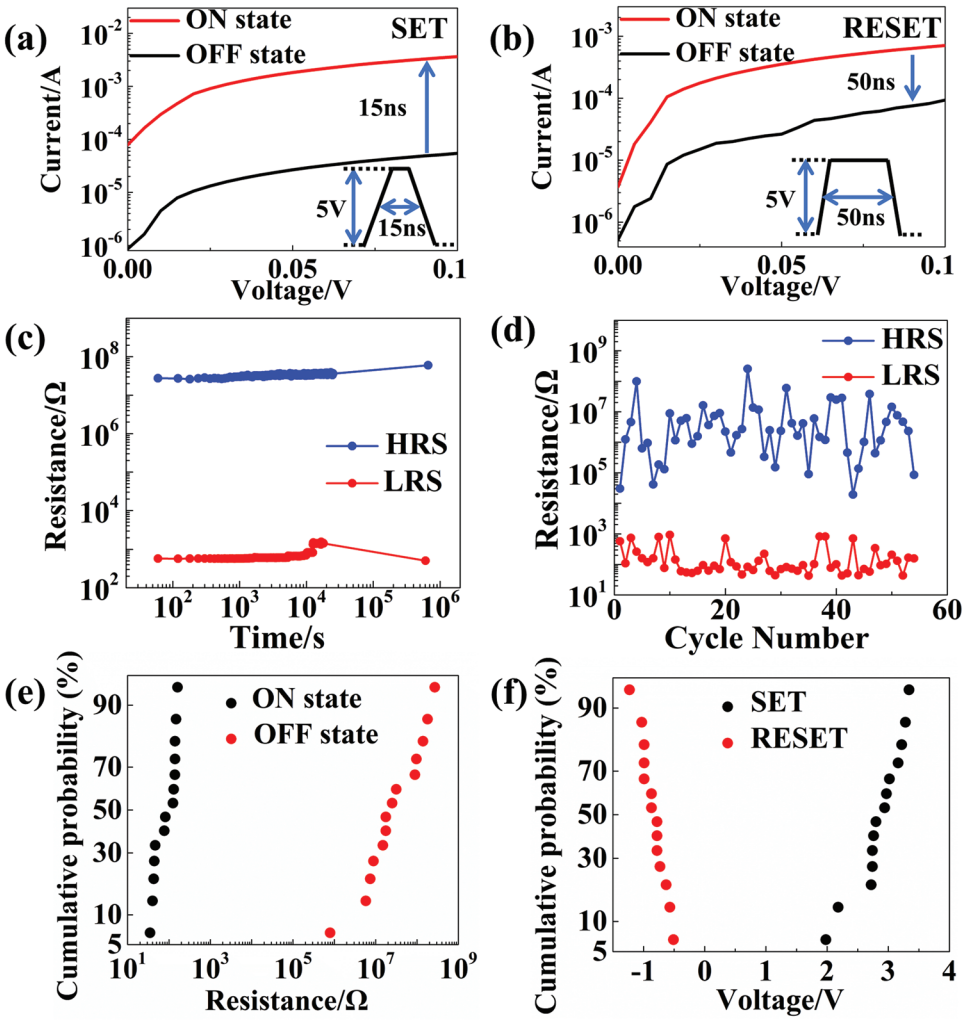

Figure 4. Pulse demonstration and reliability characterizations of monolayer nonvolatile resistance switches. a) 15 ns SET and b) 50 ns RESET pulse demonstration. c) The retention time of h-BN memory devices featuring stable retention over a week at room temperature. The resistance of HRS and LRS is determined by the current read at 0.1 V. d) Endurance of h-BN MIM device with over 50 manual DC switching cycles. e) The resistance distribution at LRS and HRS and f) the operation voltage distribution for SET and RESET are collected from 15 devices with the same lateral area of 2×2 μm^2 based on Au/h-BN/Au crossbar structure. A large minimum on/off ratio of 10^4 can be achieved with the consideration of device-to-device variability, which provides sufficient memory window even for multibit storage application and shows promising potential in RF switches.

resistance states can be retained for at least 1 week at room temperature without any degradation (see Figure 4c). For endurance, switching over 50 manual DC cycles have been achieved (Figure 4d) with more cycles expected with further studies. Device-to-device variability are presented in Figure 4e,f showing reasonable ranges for both resistance and operating voltage. Moreover, multilevel switching can be achieved under different compliance currents during SET process, enabling multibit storage and neuromorphic applications (Figure S8, Supporting Information). The comparison of monolayer h-BN atomristors with other representative 2D NVRS devices is presented in Table S1 in the Supporting Information, featuring the thinnest active layer thickness and a fast switching speed. At a nascent stage, h-BN memory cannot outperform established transitional metal oxide resistive random-access memory or phase change memory.[27,28] However, with advanced research on understanding material defects and interfaces, and optimized engineering of MIM devices, the device performance is expected to be gradually improved at the ultrathin atomic thickness.

In conclusion, we report the NVRS behavior in CVD-grown monolayer h-BN in vertical MIM configuration with 0.33 nm material thickness, a record among all NVRS materials. The h-BN atomristors show stable bipolar and unipolar resistance switching without electro-forming process, large on/off ratio (up to 10^7) and fast switching speed (<15 ns). The temperature-dependent electron transport studies and ab-initio simulation results allude to a conductive-bridge-like mechanism during switching, which is realized by the occupation of metal ions into boron vacancies, revealing fruitful interactions between metal ions and localized defects at the interface.

Experimental Section

h-BN CVD Growth on Ni Foil: CVD h-BN was synthesized by CVD by Harry Chou on Ni foil substrates, which was folded into a Ni enclosure.[29,30] Ammonia borane powder precursor was heated separately above its decomposition temperature. The precursor was carried by 5 sccm H_2 to the substrate in the furnace at 1050 °C. The process used was a carbo-thermal reduction process where another 5 sccm CH_4 gas was also flowed. The carbon does not incorporate into the h-BN, but rather helps to reduce boron oxide. After 5 min, the furnace and the methane and ammonia borane sources were shut, and the sample was cooled under 5 sccm H_2. The total pressure of the system during synthesis was roughly 200 mTorr.

h-BN Low-Chemical Vapor Deposition (LPCVD)Growth on Au Foil: LPCVD method was used to directly grow monolayer *h*-BN on Au foils, which was conducted by Zhang et al.[31] First, commercial Au foils with thickness of 25 µm were sequentially cleaned in HCl solution, acetone and distilled water for ≈10 min using ultrasonic cleaner. Further high-temperature annealing (950 °C for 5 h) in the air condition was induced to improve the crystallinity and flatness of the Au foils. Second, the pretreated foils were placed into a tube furnace chamber for the growth of *h*-BN. The chamber was pumped to 0.5 Pa and then a mixture flow of 200 sccm H_2 and 80 sccm Ar were flown in the chamber as carrier gases. After high-temperature annealing for 60 min at 1030 °C, ammonia borane vapor was mixed into the carrier gases as the h-BN feedstocks for 10 min. Finally, the temperature of chamber was naturally cooled down to room temperature.

Materials Characterization: The OM (Olympus BX51), SEM (Hitachi S-4800, 1 kV, 10 µA), XPS (Kratos Analytical Ltd. AXIS-Ultra with monochromatic Al Kα X-ray), AFM (Bruker, Dimension Icon), UNISOKU UHV-STM/STS system and Raman (Renishaw in-Via system using a 532 nm wavelength source) were employed to characterize the as-grown and transferred samples.

Device Fabrication and Characterization: For the crossbar device, BEs were patterned by electron beam lithography and then deposited by e-beam evaporation with 2 nm Cr (adhesion layer)/60 nm Au on an SiO_2/Si (285 nm) substrate. CVD h-BN was transferred onto BE from the Ni foil substrate using a poly(methyl methacrylate) (PMMA)-assisted wet transfer method. A thin layer of PMMA was spin coated onto the h-BN/Ni and then the Ni was etched away in 0.5 M ammonia persulfate solution. The PMMA/h-BN was rinsed in DI water to remove any etchant by-product prior to lifting by the target substrate with BE. The PMMA was then removed by immersing in acetone. Then, TEs were fabricated using the same process as BE. While for the litho- and transfer-free device, the growth substrate of h-BN, including Ni or Au, served as global BE. Then TE (60 nm Au without any adhesion layer) was deposited via a shadow mask. The DC characteristics of the devices based on monolayer h-BN were measured on a Cascade probe station with an Agilent 4156C semiconductor parameter analyzer under ambient conditions. Low-temperature transport was performed on a Lakeshore probe station with a Keysight B1500A semiconductor device analyzer in vacuum ambient (<1 mTorr). The pulse measurements were conducted using a Keithley 4200A-SCS parameter analyzer.

Ab-Initio Simulation: The simulation package, Atomistix ToolKit (ATK) from QuantumWise, was applied for building optimization system and electronic analysis. The electronic properties were evaluated with density-functional theory. Generalized gradient approximation was chosen as exchange-correlation energy. The density mesh cut off was 545 eV with a Monkhorst–Pack k-point sampling of $3 \times 3 \times 1$ mesh. The gold atom was set to positively or negatively charged by adding compensation charge. The systems of positive and negative gold ions substitution were optimized until the atomic force was below 0.01 eV $Å^{-1}$, and the percentage studies was performed until the atomic force was below 0.05 eV $Å^{-1}$ and the cell was transformed from hexagonal to orthorhombic for the convenient of area calculation. For energy calculation, the 5×5 supercell of h-BN sheet was constructed for the optimization process.

Supporting Information

Supporting Information is available from the Wiley Online Library or from the author.

Acknowledgements

X.W. and R.G. contributed equally to this work. This work was supported in part by the National Science Foundation (NSF) grant #1809017. The authors acknowledge use of Texas Nanofabrication Facilities supported by the NSF NNCI award #1542159. D.A. acknowledges the Presidential Early Career Award for Scientists and Engineers (PECASE) through the Army Research Office (W911NF-16-1-0277). The authors appreciate fruitful discussions with Ying-Chen Chen of UT-Austin, and Jo Wozniak of Texas Advanced Computing Centre (TACC) for 3D renderings.

Conflict of Interest

The authors declare no conflict of interest.

Keywords

2D materials, atomristor, hexagonal boron nitride, memristor, nonvolatile resistance switching

Received: October 19, 2018
Revised: January 31, 2019
Published online: February 17, 2019

[1] Q. H. Wang, K. Kalantar-Zadeh, A. Kis, J. N. Coleman, M. S. Strano, *Nat. Nanotechnol.* **2012**, *7*, 699.
[2] D. Akinwande, N. Petrone, J. Hone, *Nat. Commun.* **2014**, *5*.
[3] A. Molle, J. Goldberger, M. Houssa, Y. Xu, S. C. Zhang, D. Akinwande, *Nat. Mater.* **2017**, *16*, 163.
[4] S. Mao, J. B. Chang, H. H. Pu, G. H. Lu, Q. Y. He, H. Zhang, J. H. Chen, *Chem. Soc. Rev.* **2017**, *46*, 6872.
[5] W. N. Zhu, S. Park, M. N. Yogeesh, K. M. McNicholas, S. R. Bank, D. Akinwande, *Nano Lett.* **2016**, *16*, 2301.
[6] J. Q. Liu, Z. Y. Yin, X. H. Cao, F. Zhao, L. H. Wang, W. Huang, H. Zhang, *Adv. Mater.* **2013**, *25*, 233.
[7] C. L. Tan, Z. D. Liu, W. Huang, H. Zhang, *Chem. Soc. Rev.* **2015**, *44*, 2615.
[8] D. Son, S. I. Chae, M. Kim, M. K. Choi, J. Yang, K. Park, V. S. Kale, J. H. Koo, C. Choi, M. Lee, J. H. Kim, T. Hyeon, D. H. Kim, *Adv. Mater.* **2016**, *28*, 9326.
[9] V. K. Sangwan, H. S. Lee, H. Bergeron, I. Balla, M. E. Beck, K. S. Chen, M. C. Hersam, *Nature* **2018**, *554*, 500.
[10] C. X. Hao, F. S. Wen, J. Y. Xiang, S. J. Yuan, B. C. Yang, L. Li, W. H. Wang, Z. M. Zeng, L. M. Wang, Z. Y. Liu, Y. J. Tian, *Adv. Funct. Mater.* **2016**, *26*, 2016.
[11] L. Zhao, Z. Jiang, H. Y. Chen, J. Sohn, K. Okabe, B. Magyari-Kope, H. S. P. Wong, Y. Nishi, *IEEE International Electron Devices Meeting (IEDM)*, San Francisco, CA **2014**, pp. 6.6.1–6.6.4.
[12] C. L. Tan, H. Zhang, *Chem. Soc. Rev.* **2015**, *44*, 2713.
[13] R. J. Ge, X. H. Wu, M. Kim, J. P. Shi, S. Sonde, L. Tao, Y. F. Zhang, J. C. Lee, D. Akinwande, *Nano Lett.* **2018**, *18*, 434.
[14] M. Kim, R. J. Ge, X. H. Wu, X. Lan, J. Tice, J. C. Lee, D. Akinwande, *Nat. Commun.* **2018**, *9*.
[15] C. R. Dean, A. F. Young, I. Meric, C. Lee, L. Wang, S. Sorgenfrei, K. Watanabe, T. Taniguchi, P. Kim, K. L. Shepard, J. Hone, *Nat. Nanotechnol.* **2010**, *5*, 722.

[16] G. Giovannetti, P. A. Khomyakov, G. Brocks, P. J. Kelly, J. van den Brink, *Phys. Rev. B* **2007**, 76.
[17] L. Lindsay, D. A. Broido, *Phys. Rev. B* **2011**, 84.
[18] K. Watanabe, T. Taniguchi, H. Kanda, *Nat. Mater.* **2004**, *3*, 404.
[19] Q. H. Weng, X. B. Wang, X. Wang, Y. Bando, D. Golberg, *Chem. Soc. Rev.* **2016**, *45*, 3989.
[20] J. Lee, T. J. Ha, K. N. Parrish, S. F. Chowdhury, L. Tao, A. Dodabalapur, D. Akinwande, *IEEE Electron Device Lett.* **2013**, *34*, 172.
[21] C. B. Pan, Y. F. Ji, N. Xiao, F. Hui, K. C. Tang, Y. Z. Guo, X. M. Xie, F. M. Puglisi, L. Larcher, E. Miranda, L. L. Jiang, Y. Y. Shi, I. Valov, P. C. McIntyre, R. Waser, M. Lanza, *Adv. Funct. Mater.* **2017**, *27*, 1604811.
[22] Y. Shi, C. Pan, V. Chen, N. Raghavan, K. L. Pey, F. M. Puglisi, E. Pop, H. S. P. Wong, M. Lanza, *IEEE International Electron Devices Meeting (IEDM)*, San Francisco, CA, **2017**, pp. 5.4.1–5.4.4.
[23] J. Frenkel, *Phys. Rev.* **1938**, *54*, 647.
[24] P. Fiorenza, G. Greco, F. Giannazzo, R. Lo Nigro, F. Roccaforte, *Appl. Phys. Lett.* **2012**, *101*, 172901.
[25] A. Zobelli, C. P. Ewels, A. Gloter, G. Seifert, *Phys. Rev. B* **2007**, *75*, 094104.
[26] B. Huang, H. Lee, *Phys. Rev. B* **2012**, *86*, 245406.
[27] H. S. P. Wong, H. Y. Lee, S. M. Yu, Y. S. Chen, Y. Wu, P. S. Chen, B. Lee, F. T. Chen, M. J. Tsai, *Proc. IEEE* **2012**, *100*, 1951.
[28] S. W. Fong, C. M. Neumann, H. S. P. Wong, *IEEE Trans. Electron Devices* **2017**, *64*, 4374.
[29] A. Ismach, H. Chou, D. A. Ferrer, Y. P. Wu, S. McDonnell, H. C. Floresca, A. Covacevich, C. Pope, R. Piner, M. J. Kim, R. M. Wallace, L. Colombo, R. S. Ruoff, *ACS Nano* **2012**, *6*, 6378.
[30] A. Ismach, H. Chou, P. Mende, A. Dolocan, R. Addou, S. Aloni, R. Wallace, R. Feenstra, R. S. Ruoff, L. Colombo, *2D Mater.* **2017**, *4*, 025117.
[31] Z. P. Zhang, X. J. Ji, J. P. Shi, X. B. Zhou, S. Zhang, Y. Hou, Y. Qi, Q. Y. Fang, Q. Q. Ji, Y. Zhang, M. Hong, P. F. Yang, X. F. Liu, Q. Zhang, L. Liao, C. H. Jin, Z. F. Liu, Y. F. Zhang, *ACS Nano* **2017**, *11*, 4328.